

Ising model phase-diagram calculations in the fcc lattice with first- and second-neighbor interactions

J. M. Sanchez

Henry Krumb School of Mines, Columbia University, New York, New York 10027

D. de Fontaine

Department of Materials Science and Mineral Engineering, University of California, Berkeley, California 94720

(Received 6 August 1981)

Phase diagrams for a model fcc binary alloy with first- and second-neighbor interactions are calculated in the tetrahedron-octahedron approximation of the cluster-variation method. The calculations are carried out for two values of the ratio of second- to first-neighbor pair interactions in the range of 0 to 0.5, where the low-temperature-ordered structures occur at stoichiometries A_2B_2 , A_2B , A_3B , and A_5B .

I. INTRODUCTION

A problem of great interest in the study of the thermodynamic properties of alloys is the calculation of the associated temperature-composition phase diagram. Among the earliest attempts to obtain an order-disorder phase diagram for fcc lattices was that of Shockley¹ who, in 1938, calculated the equilibrium phase boundaries for $L1_0$ and $L1_2$ ordering (CuAu type) in the molecular field or Bragg-Williams (BW) approximation. The results of the molecular-field approximation clearly indicated the need of higher approximations for the treatment of ordering in fcc lattices. Within mean-field theories, the next approximation, namely, the Bethe or pair approximation fails even more dramatically than BW, predicting no order-disorder transition at finite temperatures.

The first encouraging result of the mean-field approach to fcc lattices came with the use of the quasichemical method of Guggenheim. Although the results of the quasichemical method are far from being satisfactory, the calculated CuAu-type phase diagram displayed most of the expected topological features.²

In 1951, Kikuchi³ proposed a variational approach, the so-called cluster variation method (CVM), which represented an appreciable improvement over the quasichemical method. Despite the fact that the CVM was, and still is, the most accurate mean-field theory available, it was not used for the calculation of order-disorder phase diagrams in fcc lattices until van Baal's work in 1973.⁴ The phase diagram obtained by van Baal was again for $L1_0$ and $L1_2$ -type ordering, with the calculations carried out in the lowest meaningful approximation of the CVM, namely, that corresponding to the nearest-neighbors tetrahedron. Since the work of van Baal, the tetrahedron approximation of the CVM has been used quite successfully

to calculate the binary CuAu⁵ and the ternary CuAu-Ag⁶ phase diagrams where ordering is also of the $L1_0$ and $L1_2$ type.

Recently, Mahan and Claro⁷ have tackled the problem of calculating a CuAu-type phase diagram by real-space renormalization-group theory. The method, however, fails to give the $L1_0$ ordered phase and it incorrectly predicts the $L1_2$ transition to be second order.

At the present time, the most reliable phase diagram in fcc systems with first-neighbor interactions is undoubtedly the one obtained by Binder⁸ via Monte Carlo calculations. There are clear and in fact not surprising discrepancies between the previous CVM calculations and the more recent Monte Carlo results, particularly away from the stoichiometric compositions. Nevertheless, the CVM calculations reproduce quite well many of the topological features of the phase diagram and, near stoichiometry, discrepancies with the Monte Carlo results are within a few percent. One would expect that including larger clusters in the CVM free energy expansion should result in yet better agreement.

Recently, the authors have used a higher level of approximation the CVM, resulting from the combination of the tetrahedron and octahedron in the fcc lattice, to calculate a prototype phase diagram for systems with first- and second-neighbor interactions.⁹ The ratio α of first- to second-neighbor pair interactions was chosen equal to 0.25 (with positive first-neighbor interaction) and thus, as it is well known from the analysis of the ground states,¹⁰⁻¹² the ordering at low temperatures is somewhat more complex than the $L1_0$ and $L1_2$ type occurring for $\alpha \leq 0$. The ground-states structures for values of α between 0 and 0.5, shown in Fig. 1, are found at stoichiometries AB , A_2B , A_3B , and A_5B . The phase diagram reported in Ref. 9 for $\alpha=0.25$ is only partially complete

since the low symmetry A_5B structure was not included in the calculations.

Although a complete Monte Carlo calculation for $\alpha=0.25$ is not yet available, Phani, Lebowitz, and Kalos¹³ have recently obtained the transition temperature at two isolated points of concentration 0.5 and 0.25. The CVM and Monte Carlo results differ, at such points, by less than 5%. In view of the discrepancies between the Monte Carlo and the CVM calculations in the CuAu-type phase diagram away from stoichiometry, it would appear safe to expect a similar behavior for values of α in the range 0 to 0.5. Nonetheless, and because of obvious computational advantages over the Monte Carlo method, it is of great interest to establish the reliability of the CVM for different levels of approximation. In order to provide the basis for comparison with future Monte Carlo simulations, we calculate here the complete phase diagrams (A_5B phase included) for α equal to 0.35 to 0.45. As we shall see, the resulting phase diagrams are relatively complex, being very sensitive to the ratio of second- to first-neighbor interactions (α).

The organization of this work is as follows. In the next section a brief review of the CVM is given. For a more detailed description of the free energy characterization, the reader is referred to Ref. 9. In Sec. III, the crystallography of the relevant ground states is described and the results of the phase diagram calculation are presented in Sec. IV.

II. CLUSTER-VARIATION METHOD

The model to be adopted here consists of a binary system with atomic species A and B occupying a rigid fcc lattice. The configurational energy will be assumed to be given by the sum of pair interactions between first and second neighbors, characterized, respectively, by constant energy parameters v_1 and v_2 . In terms of the spin operator $\sigma(p)$, which equals 1 and -1 if lattice point p is, respectively, occupied by an A or a B atom, the configurational energy is

$$E(\sigma) = \frac{1}{2}v_1 \sum_p \sum_{r_1} \sigma(p)\sigma(p+r_1) + \frac{1}{2}v_2 \sum_p \sum_{r_2} \sigma(p)\sigma(p+r_2) , \quad (1)$$

where the sums are over all lattice points p , and over first (r_1) and second (r_2) neighbors of p .

The free energy of the system can be formally obtained by minimization of the following functional¹⁴:

$$F = \sum_{\{\sigma\}} E(\sigma)X(\sigma) + k_B T \sum_{\{\sigma\}} X(\sigma) \ln X(\sigma) , \quad (2)$$

where, for a binary system with N lattice sites, the sums run over the 2^N configurations and where

$E(\sigma)$ and $X(\sigma)$ are, respectively, the energy and probability of configuration $\{\sigma\}$.

The first term on the right-hand side of Eq. (2), equal to the average energy $\langle E \rangle$, can be easily written in terms of the pair correlation $\xi_{2,r}(p) = \langle \sigma(p) \times \sigma(p+r) \rangle$. In the present approach, the pair correlations are variational parameters determined by the minimization of the free energy functional.

The key aspect of the CVM is that it approximates the entropy term in Eq. (2) by a sum of similar terms involving the probabilities for small clusters of lattice points. Such cluster probabilities will be denoted by $x_{n,s}(J,p)$, where n refers to the number of points in the cluster and where s is an index characterizing its geometry. The arrangement of A and B atoms in the cluster is specified by J , which take 2^n values for a binary system. Finally, p refers to the location in the lattice of the n,s cluster. In general, the CVM free energy functional for first- and second-neighbors interactions can be written as

$$F = \frac{1}{2}v_1 \sum_p \sum_{r_1} \xi_{2,r_1}(p) + \frac{1}{2}v_2 \sum_p \sum_{r_2} \xi_{2,r_2}(p) + k_B T \sum_p \sum_{n,s} \gamma_{n,s} \sum_{J=1}^{2^n} x_{n,s}(J,p) \ln x_{n,s}(J,p) , \quad (3)$$

where the coefficients $\gamma_{n,s}$ depend on the geometry of the lattice and on the clusters included in the approximation. A set of independent variational parameters in Eq. (3) is given by the multisite correlation functions defined by

$$\xi_{n,s}(p) = \langle \sigma(p)\sigma(p+r_1) \dots \sigma(p+r_{n-1}) \rangle , \quad (4)$$

where the angle brackets represent an ensemble average and where the set of vectors $\{r_1 \dots r_{n-1}\}$ defines the n -point cluster of type s located at lattice point p . As shown elsewhere, the cluster probabilities $x_{n,s}(J,p)$ are given by linear combinations of the multisite correlation functions.⁹

Although there is no definite criterion for deciding *a priori* which clusters should be included in the free energy expansion, a number of relatively accurate approximations for the fcc lattice are currently available. The approximation to be used here is that resulting from the combination of the regular tetrahedron and octahedron which allows for first- and second-neighbor interactions in the configurational energy.^{9,15} In the tetrahedron-octahedron (TO) approximation there are 54 correlation functions per lattice point, one for each of the subclusters of the tetrahedron and octahedron. For a detailed description of the correlations in question, the reader is referred to Ref. 9. Those clusters which appear explicitly in the free energy formula [see Eq. (3)] are: The point ($\gamma_1 = -1$); the nearest-neighbor pairs ($\gamma_{2,s} = 1$; $s = 1, 2 \dots 6$); the nearest-neighbors triangles ($\gamma_{3,s} = -1$; $s = 1, 2 \dots 8$); the regular tetrahedron

($\gamma_{4,s}=1; s=1,2$) and the octahedron ($\gamma_6=1$).

In order to carry out the minimization of the free energy functional, one must first reduce the infinite number of variational parameters in Eq. (3) to a finite set. For a given phase, the reduction in variational parameters follows from the application of all the symmetry operations of the associated space group. Thus, the use of the CVM requires a detailed knowledge of the ordered structures expected to be stable at low temperatures (ground states).

The ground states of the fcc lattice with first- and second-neighbor interactions are well known since the work of Kanamori,¹⁰ of Richards and Cahn,¹¹ and of Allen and Cahn.¹² For positive first-neighbor interactions ($v_1 > 0$) there are three distinct sets of ground-state structures occurring for different values of the ratio α of second- to first-neighbor pair interactions. For negative values of α , the lowest energy structures occur at stoichiometries $\frac{1}{2}$ and $\frac{1}{4}$. The structures in question correspond to the $L1_0(P4/mmm)$ and to the $L1_2(Pm3m)$ ordered phases. As mentioned in the Introduction, the phase diagram associated with the $L1_0$ and $L1_2$ structures has been studied in a number of different approximations for the special case of $\alpha=0$.

For values of α larger than 0.5 there are three ordered ground states at stoichiometries $\frac{1}{2}$, $\frac{1}{3}$, and $\frac{1}{6}$, the space groups of which are $R\bar{3}m$, $C2/m$, and $C2/m$, respectively. To our knowledge, no attempt has been made to calculate the phase diagram in this particular region of α .

Finally, for values of α between 0 and 0.5, the ground states are found at stoichiometries $\frac{1}{2}$, $\frac{1}{3}$, $\frac{1}{4}$, and $\frac{1}{6}$. This particular set of ground states has been named the $(1, \frac{1}{2}, 0)$ family after the point in reciprocal space where the Fourier transform of the pair potential is minimum.¹⁶ As mentioned in the Introduction, a partial phase diagram for the $(1, \frac{1}{2}, 0)$ family, not including the ground state of stoichiometry $\frac{1}{6}$, has been calculated by the authors in the TO approximation of the CVM for $\alpha=0.25$. The results of a more complete calculation will be present in Sec. IV for $\alpha=0.35$ and for $\alpha=0.45$.

III. CRYSTALLOGRAPHY OF $(1, \frac{1}{2}, 0)$ FAMILY

The unit cells for the ground-states structures of the $(1, \frac{1}{2}, 0)$ family ($0 < \alpha < 0.5$), labeled A_2B_2 , A_2B , A_3B and A_5B , are schematically shown in Figs. 1(a) through 1(d).

For the A_2B_2 structure (space group $I4_1/amd$), the vectors defining the tetragonal unit cell are, in the fcc lattice coordinates, $\vec{a}=(1,0,0)$, $\vec{b}=(0,1,0)$ and $\vec{c}=(0,0,2)$. The atomic species A and B occupy the Wickoff positions, of multiplicity 4, labeled a and b in

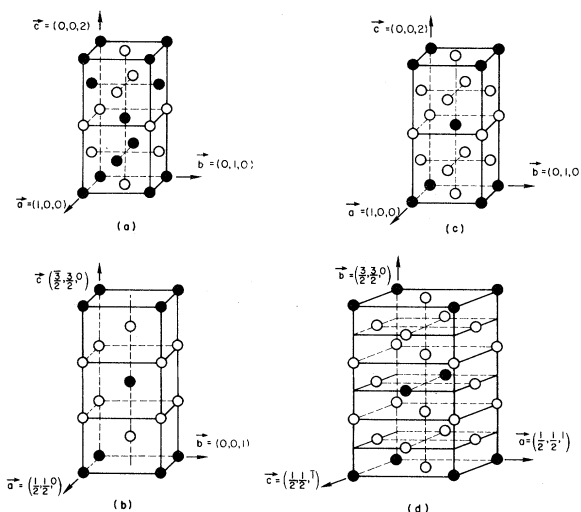


FIG. 1. Schematic unit cells for the structures of the $(1, \frac{1}{2}, 0)$ family: A_2B_2 (a), A_2B (b), A_3B (c), and A_5B (d).

the International Tables for X-Ray Crystallography.¹⁷ Thus the order parameter η for the A_2B_2 structure is one dimensional and is defined as the difference of the point correlation function $\xi_1(p)$ at each of the two Wickoff positions (a and b):

$$\eta = \frac{1}{2} [\xi_1(a) - \xi_1(b)] \quad (5)$$

In terms of the Fourier concentration spectrum for the A_2B_2 structure, the order parameter η is equal to the amplitude of a concentration wave with wave vector at the isolated symmetry point $(1, \frac{1}{2}, 0)$. By applying all the symmetry elements of the space group $I4_1/amd$ to the infinite set of cluster probabilities implicit in Eq. (3), one obtains a set of 33 independent correlation functions (or variational parameters).

The A_2B structure shown in Fig. 1(b) (space group $Immm$), of which Pt_2Mo is an example, is the highest symmetry ordered structure that can be associated with the degenerate ground state occurring at stoichiometry $\frac{1}{3}$. With respect to the fcc lattice, the vectors defining the orthorhombic unit cell [see Fig. 1(b)] are $\vec{a}=(\frac{1}{2}, \frac{1}{2}, 0)$, $\vec{b}=(0,0,1)$ and $\vec{c}=(\frac{3}{2}, \frac{3}{2}, 0)$. The two atomic species are at Wickoff positions labeled a (B atoms) and i (A atoms) of multiplicities 2 and 4, respectively.¹⁷ Thus, the long-range order parameter is again one dimensional, being defined as

$$\eta = \frac{1}{2} [\xi_1(i) - \xi_1(a)] \quad (6)$$

After applying the symmetry operations of the space group associated with the A_2B phase, there remain 46 variational parameters for the minimization of the free energy functional.

The A_3B ground state [see Fig. 1(c)] is exemplified in nature by the Al_3Ti structure (space group $I4/mmm$; structurbericht $D0_{22}$). The vectors of the tetragonal unit cell are $\vec{a} = (1,0,0)$, $\vec{b} = (0,1,0)$, and $\vec{c} = (0,0,2)$, with atoms A and B occupying three different Wickoff positions: B atoms are at Wickoff positions a of multiplicity 2 and A atoms are at Wickoff positions b and d of multiplicities 2 and 4, respectively.¹⁷ The order parameter for the A_3B phase is then two dimensional, with the two components $\eta_{1,0,0}$ and $\eta_{1,\frac{1}{2},0}$ given by

$$\eta_{1,0,0} = \frac{1}{2} [2\xi_1(d) - \xi_1(b) - \xi_1(a)] , \quad (7a)$$

$$\eta_{1,\frac{1}{2},0} = \frac{1}{2} [\xi_1(b) - \xi_1(a)] . \quad (7b)$$

The order parameters defined by Eqs. (7a) and (7b) are, respectively, the amplitudes of concentration waves with wave vectors at the isolated symmetry points $(1,0,0)$ and $(1,\frac{1}{2},0)$ in reciprocal space. The free energy minimization for the A_3B structure is carried out, in the TO approximation, with respect to a reduced set of 45 correlation functions.

The A_5B ground state is the lowest symmetry structure in the $(1,\frac{1}{2},0)$ family, with space group $C2/m$. The monoclinic unit cell shown in Fig. 1(d) is defined by the vectors $\vec{a} = (\frac{1}{2}, \frac{1}{2}, 1)$, $\vec{b} = (\frac{3}{2}, \frac{3}{2}, 0)$, and $\vec{c} = (\frac{1}{2}, \frac{1}{2}, \bar{1})$. Atoms B are at Wickoff positions a of multiplicity 2, whereas A atoms occupy Wickoff positions d, g , and h of multiplicities 2, 4 and 4, respectively.¹⁷ The three-dimensional order parameter (η_1, η_2, η_3) is defined as:

$$\eta_1 = \frac{1}{2} [\xi_1(d) - \xi_1(a)] , \quad (8a)$$

$$\eta_2 = \frac{1}{2} [\xi_1(g) - \xi_1(a)] , \quad (8b)$$

$$\eta_3 = \frac{1}{2} [\xi_1(h) - \xi_1(a)] . \quad (8c)$$

There are, in all, 76 variational parameters in the TO approximation for the A_5B phase.

IV. PHASE DIAGRAM CALCULATION

The computation of phase diagrams in the CVM centers around the minimization of the free energy functional. For each value of temperature and average concentration considered, one must numerically solve a relatively large number of nonlinear algebraic equations. The procedure is carried out for the disordered and for each of the ordered phases of interest; namely, those structures which are ground states.

For the purpose of determining phase equilibria, it is more convenient to introduce the grand potential

$$g(\mu, T) = f(\xi_1, T) + \mu\xi_1 , \quad (9)$$

where f is the minimum of the free energy functional (per lattice point), where ξ_1 is the average value of the point correlation function, and where μ is the chemical potential defined by

$$\mu = -\frac{\partial f}{\partial \xi_1} . \quad (10)$$

As prescribed by thermodynamics, the coexistence of any two phases in the temperature-chemical potential space is determined by the equality of the associated grand potentials at equal values of T and μ .

Figures 2 and 3 show the temperature-chemical potential phase diagrams for the fcc lattice, calculated in the TO approximation with the ratio α of first- to second-neighbor pair interactions equal to 0.35 and 0.45. The temperature and chemical potential in Figs. 2 and 3 are normalized by the first-neighbor pair interaction v_1 (positive). Since the alloy model of Sec. II is isomorphic to the spin- $\frac{1}{2}$ Ising model, the phase diagrams shown in Figs. 2 and 3 also describe an antiferromagnet. The chemical potential in the latter case should be taken proportional to the magnetic field.

In addition to the equilibrium phase boundaries, the phase diagrams of Figs. 2 and 3 show, in broken lines, the loci of the highest instability temperature for the disordered solid solution.¹⁶ The instability temperature, or ordering spinodal, acquires definite meaning within the realm of thermodynamics at those regions where the ordering transition is second order. Such is the case for A_3B ordering for $\alpha = 0.45$, and for A_2B_2 ordering for $\alpha = 0.35$ and large negative values of the chemical potential.

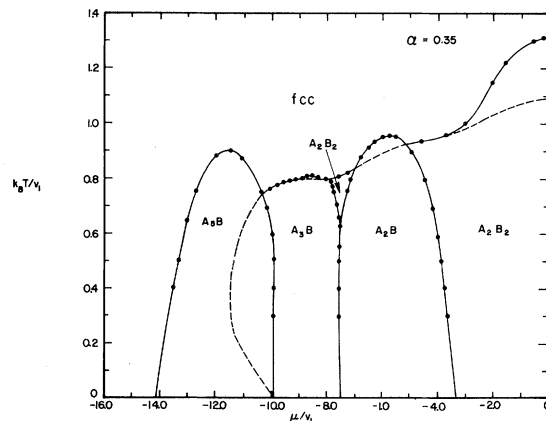


FIG. 2. Temperature-chemical potential phase diagram for $\alpha = 0.35$.

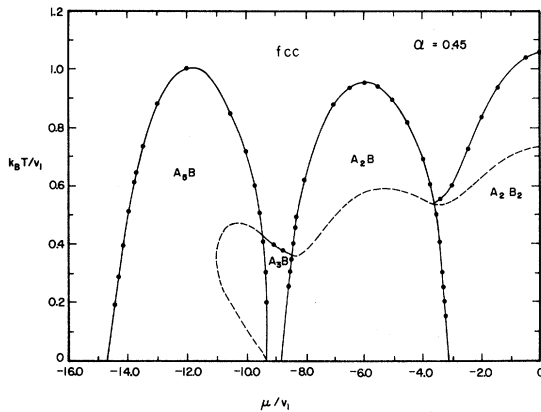


FIG. 3. Temperature-chemical potential phase diagram for $\alpha = 0.45$.

The interpretation of the ordering spinodal, which in the present case corresponds to the instability of a composition wave of wave vector $(1, \frac{1}{2}, 0)$, becomes considerably more subtle below a first-order transition. In fact it can only be interpreted in terms of nonequilibrium processes: if the disordered solid solution is rapidly quenched to a temperature below the spinodal, the ordering reaction will first proceed through the growth of the unstable composition wave. In general, such unstable composition wave will decay before the equilibrium ordered phase develops. An ordering mechanism along the lines described above appears to have been observed in the NiMo system.^{16,18}

The existence of an ordering spinodal below a first-order transition is, of course, a direct consequence of the approximate nature of the free energy. Thus the actual location of the instability in the equilibrium phase diagram is expected to be model dependent. Nevertheless, the instability loci in Figs. 2 and 3 have been included since they suggest an interesting way of rationalizing the experimental evidence in the NiMo system.

A salient feature of the phase diagrams shown in Figs. 2 and 3 concerns the relative stability of the different ordered structures as the ratio of second- to first-neighbor interactions changes. As shown in Ref. 9, the phase diagram for $\alpha = 0.25$ prominently displays the A_2B_2 and A_3B phases. When α increases in the range of 0 to 0.5, the stability field of the A_2B phases becomes larger, whereas that of the A_3B phase decreases. For $\alpha = 0.45$, the A_3B phase is seen to be stable only at very low temperatures and for a small range of chemical potentials (see Fig. 3).

The overall behavior of the phase diagram is, as expected, closely related to that of the ground-states structures for different values of α . For α approaching zero, the phase diagram should match the one obtained for α slightly negative, which only contains

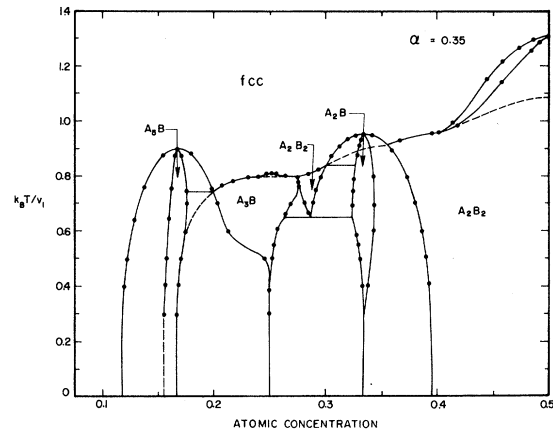


FIG. 4. Temperature-composition phase diagram for $\alpha = 0.35$.

ground states of stoichiometry $\frac{1}{2}(L1_0)$ and $\frac{1}{4}(L1_2)$. Thus the field of stability for both the A_5B and A_2B phases must become progressively smaller as α decreases, completely disappearing at $\alpha = 0$. On the other hand, and since for α larger than 0.5 the ground states occur at stoichiometries $\frac{1}{2}$, $\frac{1}{3}$, and $\frac{1}{6}$, the A_3B phase should become less stable as the limiting value of $\alpha = 0.5$ is reached from below.

The temperature-composition phase diagrams for α equal to 0.35 and 0.45 are shown, respectively, in Figs. 4 and 5. A conspicuous feature of the phase diagram for $\alpha = 0.35$ is the recurrence of the A_2B_2 phase for concentrations in the neighborhood of 0.29 and for temperatures in the range 0.64 to 0.8. The A_2B_2 phase appears in this region through a second-order transition, and it disappears at low temperatures at a eutectoid or triple point where it coexists with the A_2B and A_3B phases.

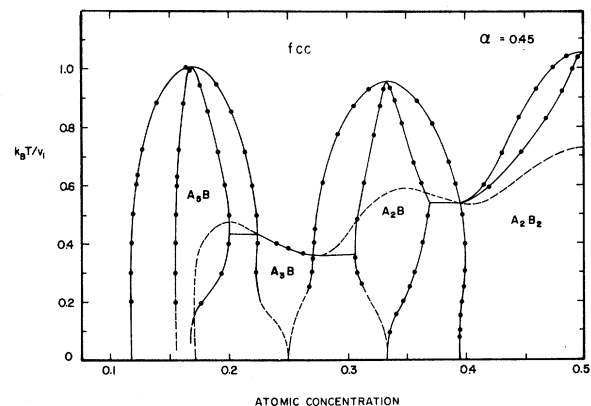


FIG. 5. Temperature-composition phase diagram for $\alpha = 0.45$.

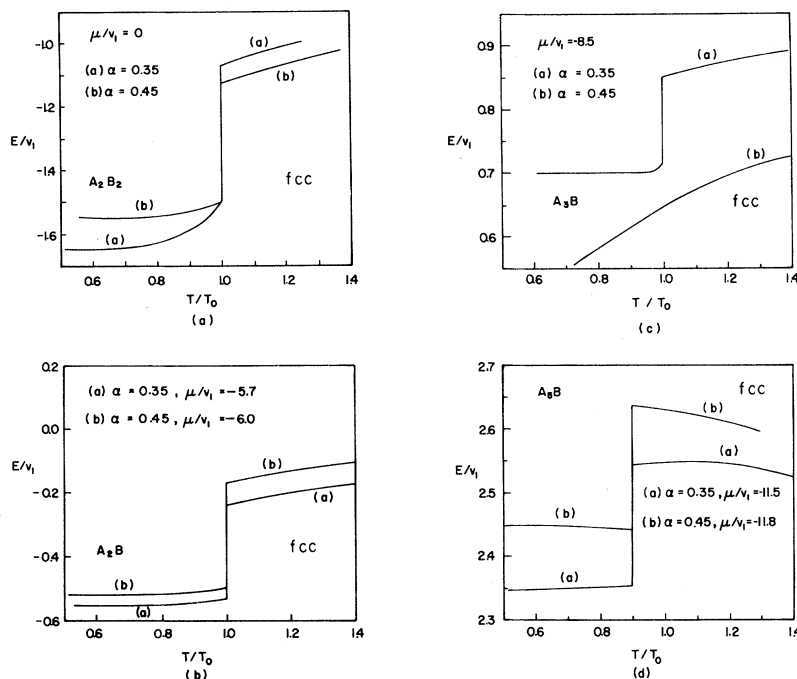


FIG. 6. Energy per lattice point vs temperature as constant field: (a) $\mu=0$; (b) $\mu=-5.7v_1$ ($\alpha=0.35$) and $\mu=-6.0v_1$ ($\alpha=0.45$); (c) $\mu=-8.5v_1$; (d) $\mu=-11.5v_1$ ($\alpha=0.35$) and $\mu=-11.8v_1$ ($\alpha=0.45$).

The Monte Carlo simulation of the CuAu-type phase diagram⁸ indicates that the CVM is significantly more accurate near stoichiometric compositions where the transitions are strongly first order. Away from stoichiometry, the transitions tend to become second order or weakly first order. In this region, small errors in the calculated free energies can significantly affect the phase diagrams since the slopes of the grand potentials at their intersection points are essentially the same.

The tendency for the transitions to become second order or weakly first order away from stoichiometry, as seen in the tetrahedron approximation for $\alpha=0$, is also observed in our calculations for α in the range of 0 to 0.5. Thus, and although we are using here a slightly improved CVM approximation (TO), the phase diagrams shown in Figs. 2–5 are expected to be more reliable near stoichiometric compositions.

Figure 6 shows the average configurational energy, normalized by the first-neighbor pair interaction v_1 , for $\alpha=0.35$ and $\alpha=0.45$. The energy has been calculated at constant field (chemical potentials), for values of μ which correspond approximately to the stoichiometric compositions of the structures of the $(1, \frac{1}{2}, 0)$ family. Except for the A_3B ordering reaction for $\alpha=0.45$, the transitions are seen to be strongly first order. The values of configurational energies shown in Fig. 6 are expected to be correct within a few percent.

V. CONCLUSIONS

The advantage of using the CVM for phase diagram calculations rests essentially on the fact that reasonably accurate results are obtained with a minimum of computational difficulty. The computational task in the CVM centers around the minimization of the free energy which, in the present case, requires the solution of approximately 30 to 70 nonlinear algebraic equations. The nature of the equations is such that the Newton-Raphson iteration method can be used quite efficiently, particularly at high temperatures. Numerical difficulties are invariably found at low temperatures, however, where some of the cluster probabilities tend exponentially to zero. Nevertheless, by taking those cluster probabilities that vanish at $T=0$ as the independent variables, one can reach temperatures of the order of $0.2T_0$, with T_0 the highest transition temperature. Since the calculations directly give the grand potential, the construction of the phase diagram does not require the laborious data analysis of the Monte Carlo simulations. Thus the method bridges the gap between the too often unsatisfactory molecular-field approximation and the computer simulation approach of the Monte Carlo method.

In evaluating the CVM results, one is usually confronted with uncertainties regarding the exact degree of accuracy that has been achieved. Fortunately, re-

cent Monte Carlo simulations have helped to clarify this point considerably. In fcc lattices at stoichiometric compositions, the CVM results agree remarkably well with the computer simulations. In fact the transition temperature for $L1_0$ ordering, calculated in the tetrahedron approximation,^{4,5} differs by about 5% from the value estimated by the Monte Carlo method.^{8,13} The results of the TO approximation, used here and in Ref. 9, are in even better agreement with the Monte Carlo calculations.¹³

Away from stoichiometry, and according to recent computer simulations by Binder,⁸ the tetrahedron approximation with first-neighbor interactions ($\alpha=0$) appear to be in serious error. It should be pointed out, however, that the tetrahedron approximation is

at the lowest meaningful level in the CVM hierarchy and, thus, one can realistically hope to narrow down the discrepancies with the Monte Carlo results by using larger cluster approximations. Nevertheless, how closely the CVM can be brought into agreement with the Monte Carlo simulations remains at the present time an open question.

ACKNOWLEDGMENTS

Programming assistance by Dr. Winston Teitler is gratefully acknowledged. This work was supported by the Army Research Office (Durham).

¹W. Shockley, J. Chem. Phys. **6**, 130 (1938).

²Y. Y. Li, J. Chem. Phys. **17**, 447 (1949).

³R. Kikuchi, Phys. Rev. **81**, 998 (1951).

⁴C. M. van Baal, Physica **64**, 571 (1973).

⁵D. de Fontaine and R. Kikuchi, in *Proceedings of NBS Workshop Applications of Phase Diagrams in Metallurgy and Ceramics, Garthersburg, June 10-12 1977*, edited by G. C. Carter (National Bureau Standards Special Publication No. 496, Vol. 2, U.S. Department of Commerce, 1978).

⁶R. Kikuchi, J. M. Sanchez, D. de Fontaine, and H. Yamachi, Acta Metall. **28**, 651 (1980).

⁷G. D. Mahan and F. C. Claro, Phys. Rev. B **16**, 1168 (1977).

⁸K. Binder, Phys. Rev. Lett. **45**, 811 (1980).

⁹J. M. Sanchez and D. de Fontaine, Phys. Rev. B **21**, 216 (1980).

¹⁰J. Kanamori, Prog. Theor. Phys. **35**, 66 (1966).

¹¹M. S. Richards and J. W. Cahn, Acta Metall. **19**, 1263 (1971).

¹²S. M. Allen and J. W. Cahn, Acta Metall. **20**, 423 (1972).

¹³M. K. Phani, J. L. Lebowitz, and M. H. Kalos, Phys. Rev. B **21**, 4027 (1980).

¹⁴T. Morita, J. Phys. Soc. Jpn. **12**, 753, 1060 (1957); J. Math. Phys. **13**, 115 (1972).

¹⁵J. M. Sanchez and D. de Fontaine, Phys. Rev. B **17**, 2926 (1978).

¹⁶D. de Fontaine, Acta Metall. **23**, 553 (1975).

¹⁷*International Tables for X-Ray Crystallography, Symmetry Groups*, edited by N. F. M. Henry and L. Lonsdale (Kynoch, Birmingham, 1952), Vol. I.

¹⁸P. R. Okamoto and G. Thomas, Acta Metall. **19**, 825 (1971).